STUDIES OF SILICON PN JUNCTION SOLAR CELLS

by

Fredrik A. Lindholm, Principal Investigator
Department of Electrical Engineering
University of Florida
Gainesville, Florida 32611

FINAL TECHNICAL REPORT
covering the period June 24, 1974 - July 23, 1975

prepared for

National Aeronautics and Space Administration
NASA Lewis Research Center
NASA grant NSG-3018

STUDIES OF SILICON PN JUNCTION SOLAR CELLS

by

Fredrik A. Lindholm, Principal Investigator
Department of Electrical Engineering
University of Florida
Gainesville, Florida 32611

FINAL TECHNICAL REPORT
covering the period June 24, 1974 - July 23, 1975

prepared for

National Aeronautics and Space Administration
NASA Lewis Research Center
NASA grant NSG-3018

e-a

FOREWORD

The author wishes to call attention to the contributions to the studies reported here made by the persons listed in Appendix C. He also wishes to acknowledge that M.P. Godlewski of the NASA Lewis Research Center provided technical assistance in various phases of the research. C.T. Sah first suggested to NASA the possibility of placing this grant research at the University of Florida, and afterwards helped make the arrangements and formulate the technical plan of the research.

F. A. Lindholm
Gainesville, Florida

TABLE OF CONTENTS

SUMMARY

Silicon pn junction solar cells made with low-resistivity substrates show poorer performance than traditional theory predicts. The purpose of the research sponsored by grant NSG-3018 is to identify and characterize the physical mechanisms responsible for this discrepancy. Attention concentrates on the open-circuit voltage in shallow-junction cells of 0.1 ohm-cm substrate resistivity.

For such cells we have considered from a theoretical vantage point the multitude of possible mechanisms that can occur in silicon devices. We have found that two mechanisms are likely to be of main importance in explaining the observed low values of open-circuit voltage: (1) recombination losses associated with defects introduced during junction formation; and (2) inhomogeneity of defects and impurities across the area of the cell. To explore these theoretical anticipations, we have designed and fabricated various diode test structures and have constructed measurement configurations for characterizing the defect properties and the areal inhomogeneity. Preliminary experimental findings were made during the period of the grant, and experimental studies now continue under a renewal of grant support.

I. INTRODUCTION

In the twenty years since the first realization of a silicon solar cell in 1954 by Chapin, Fuller and Pearson at the Bell Telephone Laboratories [1], substantial research, development and manufacturing efforts have been spent to improve efficiency [2,3] and radiation resistance [4] for space applications. The design of commercial silicon solar cells for space applications has been stabilized to n on p, 10 ohm-cm silicon base material of 2x2 cm^2 area. At present, the most advanced commercial solar cells now in production yield about 13% efficiency, 39 mA/cm^2 short circuit current and 585 mV open circuit voltage under 140 mW/cm^2 AMO solar illumination.

Shockley and Queisser [5] have shown that the intrinsic limits of the silicon solar cell efficiency is about 30% with an open-circuit voltage of about 840 mV. In the idealized case they proposed, all loss mechanisms are neglected except the intrinsic loss due to interband radiation recombination of electron-hole pairs. A semi-empirical extrapolation by Shockley and Queisser gave an extrinsic efficiency of about 22%. Taking into account the various losses more quantitatively, other workers have provided different estimates of the maximum efficiency: 22% by Wolf [2] and 18% by Brandhorst [3]. Both predict a corresponding open-circuit voltage

of about 710 mV when the silicon substrate resistivity is reduced below 0.1 ohm-cm.

Hence comparison of these estimates against the performance of commercial solar cells demonstrates a disagreement of nearly a factor of two in efficiency and of 100 to 150 mV in open-circuit voltage. Moreover, these theoretical limits have yet to be achieved in any experimental devices. For example, recent work shows that the open-circuit voltage saturates at about 600 mV as substrate resistivity is reduced to 0.1 ohm-cm [3].

This study seeks understanding of the physical mechanisms responsible for these discrepancies between experimental observation and theoretical estimate. In particular, to the present, we have concentrated most effort toward understanding the open-circuit voltage in shallow-junction cells with 0.1 ohm-cm substrate resistivity. The interest here derives from three considerations: first, the curve fill factor and the short-circuit current are thought to show better agreement between theory and experiment for these cells than does the open-circuit voltage [6,7]; second, it is believed [6] that much larger improvements are possible in open-circuit voltage than in either fill factor or short-circuit current; and, third, experimentation [6,7] suggests that performance as a function of substrate resistivity peaks for cells having resistivities of approximately 0.1 ohm-cm.

The major technical findings and other aspects of progress made during this year of grant support are presented in the following sequence.

In Section II, we summarize our theoretical anticipations about which of the multitude of possible physical mechanisms occurring in silicon junction devices predominate in producing the discrepancy here between theory and experiment. The detailed study from which these conclusions are drawn appears in Appendix A.

This study suggests that two mechanisms are likely to be of main importance: (1) recombination losses associated with defects introduced during junction formation; and (2) inhomogeneity of defects and impurities across the area of the cell. These mechanisms were among those suggested initially by Sah as likely candidates for study under this grant. In Section III, we describe the various diode test structures we have designed and fabricated and the measurement configurations we have constructed to characterize defect properties and areal inhomogeneity. In addition, we report preliminary experimental findings.

Section IV describes future plans for the research.

II. RECOMBINATION LOSSES AND AREAL INHOMOGENEITY

As was noted in the previous section, the expectation of good performance has prompted interest in solar cells with highly-doped substrates. As an example of these expectations, consider from a physical standpoint the open-circuit voltage. Open-circuited conditions imply no current at the terminals. To satisfy this constraint, an opposing component of current must arise to balance the photogenerated component. In the traditional theory, this balancing (dark) current derives from a lowering of the potential barrier at the junction, which allows excess charge to flow into the *substrate (base)* where it accumulates sufficiently to sustain the dark current. To the first order, the potential barrier lowers by an amount equal to the open-circuit voltage. The more highly doped is the substrate, the greater is the barrier height at equilibrium; and so the more it must lower to produce the dark current. Thus arises the expectation that open-circuit voltage will increase with increased doping of the substrate.

Contrary to this expectation, however, is the increased significance of regions near the surface that accompanies greater doping in the substrate. This arises for the following reason. The greater the substrate doping, the greater is the

lowering of the potential barrier. Consequently, the greater is the proportion of the excess charge accumulating in the junction space-charge region and in the quasi-neutral diffused layer (emitter) relative to that accumulating in the base.

Thus, as substrate doping increases, the physical mechanisms occurring in the emitter and in the space-charge region gain significance. Many different mechanisms, traditionally ignored, occur in these regions of high doping and high impurity gradients. That the traditional theory fails to agree with experiment suggests these mechanisms need study.

A major problem in understanding the operation of highly-doped cells lies in determining which of the mechanisms are dominant and which may be neglected. A second problem, relating to design, lies in controlling both the dominance and the magnitude of the phenomena via controlling the device structure and the steps used in fabrication, particularly during junction formation.

The issue of dominance among physical mechanisms is the subject of the theoretical study reported in Appendix A. Here, in the present section, we summarize the main conclusions deriving from this study. We dispense with most references in this section; the references for Appendix A are listed separately from those for the rest of the report, allowing Appendix A to be read as a self-contained unit. Appendix A deals wholly with a one-dimensional model of the solar cell;

in the present section, we suggest the significance of another mechanism whose consideration produces a three-dimensional model of cell behavior.

UNDERSTANDING REACHED ABOUT DOMINANT MECHANISMS: To examine the issue of dominance among the high-doping mechanisms, we have divided them into two broad categories:

1. *Gap shrinkage*, as produced, for example, by band tailing, impurity-band widening and impurity misfit; and
2. Altered *interband transition (recombination) rates* arising from Auger-impact or Shockley-Read-Hall (SRH) processes or from electronic tunneling via defects.

Which of these mechanisms predominates depends, in general, on the physical make-up of the device, on environmental conditions such as temperature, and on the aspect of cell performance of interest.

In this generality we have given only qualitative indications about the dominance of the mechanisms. To provide a *quantitative* illustration, we have taken a concrete example: a phosphorous-diffused n+p cell, junction depth 0.25 microns, impurity grade constant 10^{23} atoms/cm^4, substrate resistivity 0.1 ohm-cm. Further our attention has centered on the measured open-circuit voltage at 300°K.

To analyze this device, we have extended the traditional analytical theory of silicon solar cells to enable inclusion of the high doping mechanisms. Of these mechanisms, we have concluded that gap shrinkage, taken alone in a one-dimensional

model, falls far short of explaining the measured open-circuit voltage. To fit the data, a gap shrinkage of 0.23 eV would be required for impurity concentrations only slightly higher than 10^{18} cm^{-3}, which compares to our upper-bound estimate of 0.07 eV for such concentrations. From a physical standpoint, we predict gap shrinkage to be small because minority carriers can exist in sizable numbers in the dark cell only where the doping is relatively small. This is one of the main consequences of the piecewise linear-junction approximation used in our analysis, as contrasted with the step-junction model customarily used in the analysis of solar cells.

Of all the *one-dimensional* mechanisms considered, we have proposed the *recombination processes associated with defects created during junction formation* to be the most likely candidates to explain the open-circuit voltage experimentally observed. From a theoretical argument based on the law of mass action combined with neutrality, we find a first approximation for the spatial dependence of the defects near the surface: that the defect density rises in proportion as the rth power of the shallow-impurity density. To bring the open-circuit voltage predicted by our theory into agreement with that observed experimentally requires that the exponent r take values between below 2 to about 4, the uncertainty resulting from certain uncertainties about structure and processes that are discussed in Appendix A. The value r=2 corresponds to di-vacancies or other simple

configurations of the defects; higher values of r imply more complex configurations.

Our ultimate focus in Appendix A on the spatial dependence of the defect density came through elimination of the dominance of the other mechanisms named previously, including gap shrinkage; nonetheless, we anticipate another mechanism may rule, at least in part, many aspects of behavior of low-resistivity cells.

We have previously considered a one-dimensional model of the cell, the only coordinate of interest having been that measuring the distance from the surface. But the solar cell is a large-area device, and inhomogeneities across this area could play a significant role in governing the performance. In particular, we note the existence of a *spatial distribution of impurity clusters,* thermodynamically stable, occurring in the diffused layer [8]. This inhomogeneity may result, in part, from inescapable statistical fluctuations and, in part, from man-made contributions that could be minimized.

Combined with the one-dimensional model advanced in Appendix A, consideration of the effects of this *areal inhomogeneity* gives a three-dimensional characterization of the behavior of solar cells. Thus one can systematically view the influence of the one-dimensional mechanisms discussed in Appendix A in the context of inhomogeneity across the area of the cell. We stress that the overall effect on behavior is not a simple average over the area of the cell. Rather,

certain of the mechanisms are much emphasized, for example, in a region of large-impurity concentration due to clustering. An example is gap shrinkage, which enters as an exponent in determining cell properties in a localized region; another example is the associated increased defect density and the increased recombination rates corresponding to it. Viewing the overall solar cell as a collection of sub-cells roughly in parallel one with another, we can see that those sub-cells with relatively high doping and defect density can severely degrade the performance of the device. Hence the *areal-inhomogeneity mechanism* could play a dominant role and establish a basic limitation on the performance obtainable.

For the cell under study, therefore, we anticipate on theoretical grounds that two mechanisms may likely combine to yield the observed open-circuit voltage: (1) increased recombination rates near the surface; and (2) areal inhomogeneity. The experimental studies discussed in the following section are designed to assess these theoretical anticipations.

III. EXPERIMENTAL STUDIES

The intent in the experimental phase of the program is to test and guide the theoretical anticipations. In particular, the immediate concern is whether the discrepancy between measured and predicted open-circuit voltage in 0.1 ohm-cm cells arises mainly from the two contributors singled out in Section II: areal inhomogeneity [8] and recombination losses, especially those introduced during junction formation [9].

The general plan of the experimentation involves several parts. To study the recombination losses, we fabricate n-on-p and p-on-n diodes, made with small area to de-emphasize the contribution of areal inhomogeneity on device performance. The current-voltage characteristics are measured with the effects of surface channels minimized by the application of voltage to an MOS guard ring. These characteristics are studied for their relation, on the one hand, to the open-circuit voltage, and, on the other hand, to the parameters describing the defect centers. The open-circuit voltage is measured by use of a special mask designed to let light penetrate a major portion of the surface area of the diode. The parameters of the defects (including the densities, activation energies, thermal emission rates and

their spatial dependencies) are measured by capacitance-transient and related methods due to Sah and his co-workers [9-12]. By applying these methods to Schottky-barrier diodes of appropriate structure, one may characterize the defects present before junction formation, and, hence, infer the defects and the defect properties deriving from the processing used in pn junction formation.

To study areal inhomogeneity, we routinely map the current-voltage characteristics over the area of wafers that are processed. This is done by making measurements on small-area (~ $10^{-2}cm^2$) diodes scribed from a large-area (1.25" diameter) wafer. On these small-area devices, one can also measure the defect properties and the photo-voltage, and thus secure an areal mapping of many parameters that influence cell behavior. Alternatively, one can map the photo-voltage by probing before the wafer is scribed [13].

Two aspects of the processing are noteworthy. First, for surface preparation, we have built a tilted, teflon beaker, which rotates by a speed-controlled motor. The beaker enables a chemical polishing of silicon wafers that reduces the damage present on the surface. Second, we have devised processing, including diffusions, for fabrication with temperatures never exceeding 900°C. The intent here is to study devices with low defect densities, made by processing similar to that employed in conventional solar-cell fabrication.

Preliminary experimental findings on both np and pn devices showed good characteristics of the small-area diodes made on 0.1 ohm-cm substrates. Saturation current densities of about 10^{-11} Amperes/cm^2 and slope factors of about 1.1 were commonly seen. The experimental configurations for the transient-capacitance measurements were built and shown to work. By use of a tungsten lamp, we secured an indication of the open-circuit voltage on the small-area structures; 590 millivolts was not uncommon, which correlated well with predictions based on the observed dark-current characteristics joined with an estimate of the short-circuit current. The mappings revealed considerable areal inhomogeneity of the parameters describing the dark current and of the open-circuit voltage. This suggests the presence of a man-made contribution to the inhomogeneity.

The effort spent during this first year of grant support has put us in a good position for systematic and detailed experimental studies during the year of renewed support.

IV. FUTURE PLANS

During this period of support, we spent much effort trying to sort, on theoretical grounds, the prime contributors to the low experimental open-circuit voltage from among the multitude of different phenomena that occur in silicon devices. Section II sets forth the conclusions deriving from this effort: areal inhomogeneity and recombination losses near the surface are the likely prime contributors for the cell under study.

In the immediate future, our efforts will concentrate on an experimental assessment of these theoretical anticipations. As is implied in Appendix A, to enable such an assessment requires first filling the present gaps in understanding about the recombination losses in substrates of 0.1 ohm-cm resistivity, including the total absence of information about the spatial dependence of the lifetime. Hence our initial attention will focus on characterizing the defect properties in the substrate produced by the processing used in pn junction formation. For this study, the decreasing sensitivity of the transient-capacitance methods with increased substrate doping may pose experimental problems, which will require special experimental strategies.

In the farther future, still concentrating on cells with 0.1 ohm-cm substrate resistivity, we plan to examine further

the role of the recombination losses and other phenomena occurring in the highly-doped emitter region. Throughout, we intend to monitor the areal inhomogeneity. Open-circuit voltage will continue to be the main concern.

In the far future, we foresee an engineering phase of this study. This involves a systematic linking of the defect properties, the areal inhomogeneity, and whatever other physical mechanisms may emerge significant to the processing used in fabrication. The intent is that the scientific understanding gained shall underlie the development of better solar-cell performance.

REFERENCES

1. D.M. Chapin, C.S. Fuller and G.L. Pearson, J. Appl. Phys., v. 25, 676 (1954).

2. M. Wolf, Advanced Energy Conversion, v. 11, 63 (1971).

3. H.W. Brandhorst, Jr., 9th Photovoltaic Specialists Conference Record, 1 (1972).

4. M. Wolf and G.J. Brucker, Adv. Energy Conversion, v. 11, 75 (1971).

5. W. Shockley and H.J. Queisser, J. Appl. Phys., v. 32, 510 (1961).

6. H.W. Brandhorst and M.P. Godlewski, private communication, August 1974, and High Efficiency Silicon Solar Cell Meeting NASA-Lewis Research Center, November 1974.

7. P.A. Iles and S.I. Soclof, 11th Photovoltaic Specialists Conference Record, 75CH0948, 19 (1975).

8. W. Shockley, Solid State Electronics, 2, 35 (1961).

9. C.T. Sah and C.T. Ulang, J. Appl. Phys., v. 46, 1767 (1975).

10. C.T. Sah, L. Forbes, L.L. Rosier and A.F. Tasch, Solid-State Electronics, v. 13, 759 (1970).

11. C.T. Sah, W.W. Chan, H.S. Fu and J.W. Walker, Appl. Phys. Lett., v. 20, 193 (1972).

12. C.T. Sah and J.W. Walker, Appl. Phys. Lett., v. 22, 384 (1973).

13. At NASA Lewis Research Center, Cleveland, M.P. Godlewski has done this kind of mapping on one of our wafers.

*APPENDIX A: DETAILED CONSIDERATION OF THE ONE-DIMENSIONAL PHYSICAL MECHANISMS**

INTRODUCTION

Recent work [1,2] based on the traditional analysis of the silicon junction solar cell predicts an improvement in performance as the substrate doping is increased. But, as noted by Brandhorst [1], experiment failes to agree with theory. For example, measured open-circuit voltage peaks at a substrate resistivity of approximately 0.1 ohm-cm, and shows a maximum value of 610 mV for this resistivity [3], about ten to fifteen per cent below the predicted value [3].

Two possible sources of such disagreements are apparent. First, they may originate in the approximations made in traditional analysis; and numerical solution by computer can help identify this kind of difficulty and remedy it. This is the approach and main focus of the recent work of Fossum [4] and of Dunbar and Hauser [5,6]. Second, however, the disagreements may partly owe their origin instead to the neglect in traditional analysis of certain physical mechanisms accompanying high doping. This possibility is the subject here.

Our intent here is to describe mechanisms ignored in the customary view of cell operation, and to indicate the degree to which they can influence solar-cell characteristics. These

---

* This Appendix derives from part of the contents of the paper: F. A. Lindholm, et al., Record of Eleventh IEEE Photovoltaic Specialists Conference, pp. 3-12, (1975). Though the general conclusions of the two works agree, the Appendix contains several noteworthy additions and alterations.

mechanisms all arise from high doping; and some can substantively determine the kinetics of holes and electrons in the highly-doped diffused layer and in the junction space-charge region. For the most part, the physical mechanisms to be discussed tend to degrade the performance of solar cells. Hence they impose fundamental limitations on the performance obtainable.

As background for our treatment, we begin with a generalization of the customary view of solar-cell operation, with emphasis given to the origin of the open-circuit voltage. Next we propose the additional mechanisms and comment qualitatively on their relation to temperature and to the physical make-up of the cell. Then follows an extension of the traditional analysis and a comparison to experiment. Thus, for a one-dimensional model, we indicate which of the additional mechanisms dominate in determining the open-circuit voltage at 300°K of a cell with 0.1 ohm-cm substrate resistivity.

A GENERALIZED VIEW OF TRADITIONAL ANALYSIS

In the traditional method of analysis, as illustrated in Figure A-1, the cell is sectioned into three regions: the quasi-neutral portion of the substrate (or the base), the quasi-neutral portion of the diffused layer (or the emitter), and the junction space-charge region (or the SCR). Further, one regards the current density at the terminals as the superposition of two oppositely directed components,

$$J = J_D - J_L \qquad (1)$$

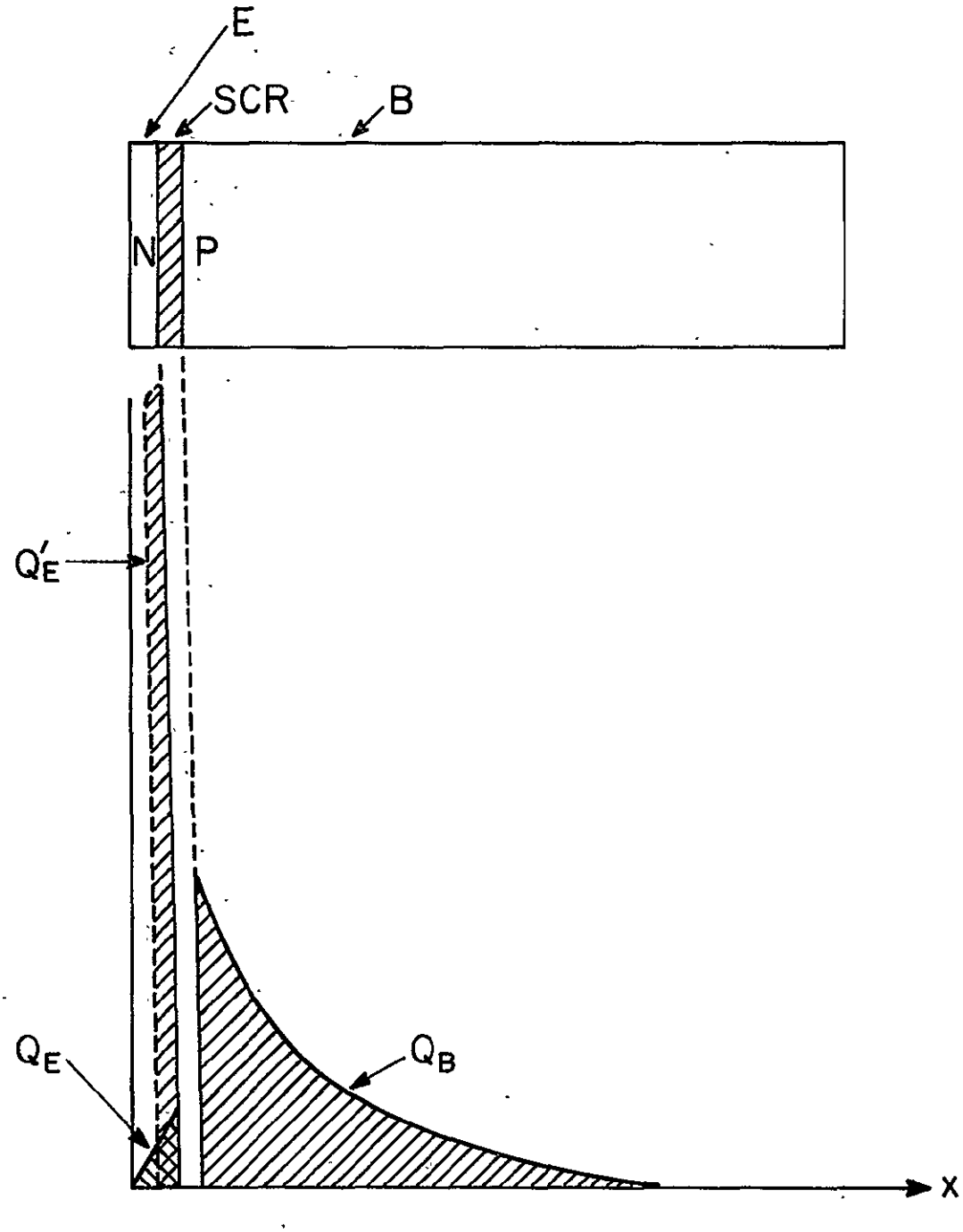

Fig. A-1 Qualitative sketch of mobile charges in dark cell, suggesting dominance of Q_B, as in traditional theory. Charge Q'_E anticipates one high-doping effect. Charge Q_{SC} is not shown.

in which J_L denotes the total spectral current density generated by the solar illumination, and J_D denotes the dark current density that would occur in the absence of illumination. Traditional analysis, as reviewed by Brandhorst [1] and Stirn [7], then bases the determination of J_D on a step-junction model and on simple diffusion theory. Here we avoid these idealizations by a more general view which, as is shown later, enables the inclusion of high-doping mechanisms.

We regard J_D as the sum of three components:

$$J_D = J_B + J_{SCR} + J_E \ . \tag{2}$$

We think of each component as deriving from the recombination-diffusion-drift kinetics of the mobile carriers in the three regions of the device, and thus regard each as the ratio of an excess mobile-carrier charge to a time constant pertaining to the region under consideration. Hence,

$$J_B = Q_B/\tau_B \ , \tag{3}$$

$$J_{SCR} = Q_{SCR}/\tau_{SCR} \ , \tag{4}$$

$$J_E = Q_E/\tau_E \ . \tag{5}$$

Figure A-1 conveys this view of the origin of the dark current. Depending on the process dominating the kinetics of the mobile carriers, the time constant will often have the physical interpretation either of a lifetime or of a drift-diffusion (transit) time or of a combination of the two. *The view expressed in Eqns. (3)-(5) is general, for a one-dimensional model, independent of the doping profiles of the mechanisms controlling cell behavior.*

Traditional analysis leads to the conclusion that J_B constitutes nearly all of the dark current density J_D at $300^{\circ}K$; that is, for

open-circuited conditions,

$$J_D \simeq J_B \tag{6}$$

Figure A-1 pictures the reason for this. The thickness of the base region by far exceeds that of the emitter or the junction space-charge regions, and consequently the charge Q_B apparently much exceeds Q_E or Q_{SCR}. Hence the base current will tend to predominate provided one supposes, as is customary, practically equal lifetimes in the three regions and a sufficiently large drift time for the emitter.

The traditional analysis* then models the dark current density using Shockley's diode theory [8]:

$$J_D \simeq J_O[\exp(qV/kT) - 1] = J_O \exp(qV/kT) \tag{7}$$

Here J_O denotes the saturation current density, which is proportional to the diffusion length L_B and is inversely proportional to the doping of the base N_B:

$$J_O = \frac{qL_B n_i^2}{\tau_B N_B} = \frac{q\sqrt{D_B} n_i^2}{\sqrt{\tau_B} N_B} \tag{8}$$

From Eq. (7) and (8) it follows that

$$Q_B \simeq \frac{qL_B n_i^2}{N_B} \exp(qV/kT) \tag{9}$$

---

* Shockley's theory [8] applies to an idealized p-n junction. Actual junctions show a current deriving from net recombination in the quasi-neutral regions that varies in proportion as $\exp(qV/mkT)$, in which m often is as much as ten or twenty per cent greater than unity. Inclusion of $m \neq 1$ in the arguments presented here causes no substantive change, however; and thus, for simplicity of discussion, we assume m=1 throughout.

which is the charge of the minority carriers in the base appearing in Eq. (3) and illustrated in Figure 1. In the notation used above, V stands for the applied potential across the junction space-charge region, and the other symbols have their usual meanings.

This conception of solar-cell operation enables an easy interpretation of the open-circuit voltage V_{OC}. To conform to open-circuited conditions, the minority charge in the base Q_B must rise until J_B is large enough to exactly balance J_L. This requires the applied component of the barrier potential to rise until it reaches

$$V_{OC} \cong kT/q \ \ell n\{J_L/J_O\} \tag{10}$$

in the forward direction. Examination of Figure A-1 and of Eqs. (8) - (10) shows that two factors compete to control V_{OC} as the substrate doping N_B increases. On the one hand, an increase in N_B tends to depress the boundary value of the minority carriers, and thus V_{OC} must increase to let more minority carriers flow into the base. On the other hand, empirical evidence exists that the lifetime drops [9] as doping increases, which demands less Q_B to constitute a given J_B; this tends to decrease V_{OC}. In the traditional theory, however, the first tendency dominates and V_{OC} is predicted to increase as doping rises [1,2].

Having established this background, we can now pinpoint flaws in the traditional method of analysis that may help explain its large predicted values of V_{OC} for highly-doped cells. First, recall that J_E and J_{SC} were neglected in comparison with J_B. Their presence in significant values could by itself explain the disagreement between experiment and theory. This one can see mathematically from Eq. (10). Or, one can view this from a more physical standpoint, using Figure A-1. Note that the presence of significant excess currents J_E or J_{SCR}, and hence of significant values of Q_E and Q_{SC}, diminishes the value of Q_B needed to balance J_L. Since according to Eq. (9), Q_B depends exponentially on V_{OC}, the presence of excess currents will therefore depress V_{OC}.

But Figure A-1, which is scaled for a substrate of ordinary doping, suggests that the excess currents are wholly negligible. What changes occur with high doping that give rise to sizable values of J_E or J_{SCR}? One such change arises from the observed drop in lifetime in the substrate [9] as substrate doping increases.* This, for example, tends to give J_{SCR} greater importance. But other changes occur too. As one can see from Eqs. (3) - (5), any mechanisms accompanying high doping that increase Q_{SCR} or Q_E (as suggested by the dashed shape in Figure A-1) or that decrease the corresponding time constants can produce sizable excess currents, and can contribute to the cell performance seen experimentally. Many such mechanisms exist, and these are discussed in the following section.

---

* The processing associated with junction formation might also affect the lifetime in the base. The experimental studies described in Section III address this question, among others.

ADDITIONAL PHYSICAL MECHANISMS

The traditional analysis can be viewed from another vantage point, which enables a concise summary of the physical mechanisms it contains. As we have noted, the traditional analysis uses Shockley's theory of the pn diode [8]. Hence, fundamentally, it relies on the equations underlying Shockley's analysis, which are:

$$\vec{J}_N = qD_n\nabla N + q\mu_n\vec{E}N \tag{11}$$

or

$$\vec{J}_N = -q\mu_n\nabla\phi_N \tag{11a}$$

$$\vec{J}_P = -qD_p\nabla P + q\mu_p\vec{E}P \tag{12}$$

or

$$\vec{J}_P = -q\mu_p\nabla\phi_P \tag{12a}$$

$$\vec{J} = \vec{J}_N + \vec{J}_P \tag{13}$$

$$0 = \frac{1}{q}\nabla\cdot\vec{J}_N + G_{EXT} - R_N \tag{14}$$

$$0 = -\frac{1}{q}\nabla\cdot\vec{J}_P + G_{EXT} - R_P \tag{15}$$

$$-\nabla^2\phi = \nabla\cdot\vec{E} = \frac{q}{\varepsilon}(N-P+N_{AA}-N_{DD}) = \frac{\rho}{\varepsilon} \tag{16}$$

These equations, joined with the auxiliary relations,

$$N = n_i \exp[q(\phi-\phi_N)/kT] \tag{17}$$

$$P = n_i \exp[q(\phi_P-\phi)/kT], \tag{18}$$

constitute the starting point not only for the traditional analysis but also for the computer studies of cell operation now beginning to appear [4-6].

The first of these equations expresses the electron current density $\vec{J}_n$ as the sum of a diffusion component, proportional to

the gradient of the density n of mobile electrons, and of a drift component, proportional to the electric field $\vec{E}$. The constants of proportionality involve the mobility μ_n and the diffusitivity D_n, together with the magnitude of the electron charge q. In Eq. (11a) appears an equivalent way of expressing the electron current density, in terms of the gradient of the quasi-Fermi level ϕ_N of electrons. Eqs. (12) and (12a) are the counterparts for the mobile holes; and Eq. (13) expresses the total current density as the sum of electron and hole components. By Eqs. (14) and (15), the continuity equations, one acknowledges that the time rate of change of mobile carriers within an infinitesimal (but macroscopic) volume arises from two sources: from the rate of flow into the volume and from the net rate $(G_{EXT} - R)$ of generation within the volume. Eq. (16) is the Poisson equation that determines the electric field in terms of the charge density. The components of the charge density include the densities, N_{AA} and N_{DD}, of the acceptor and donor impurity ions. The dielectric permittivity ε enters as usual.

In the analysis of solar cells, the term G_{EXT} describing external generation receives special attention; it gives rise to the total spectral current density J_L generated by the illumination. The recombination rates R_N and R_P are customarily modeled either simply in terms of carrier lifetime or by assuming a single SRH defect center lying near mid-gap [10,11]. As we have noted, the traditional analysis treats the lifetime as spatially independent, though its dependence on doping in the substrate [9] has recently been included [3].

Eqs. (11) - (18) constitute the physical mechanisms conventionally included in the analysis of solar-cell operation. By computer solution, one can take account of the effects of these mechanisms on cell operation with near exactness. The method of traditional analysis obscures their effects through the idealizations made, though it can give useful physical insight.

We now discuss additional physical mechanisms, not customarily included, which can occur in highly-doped cells and can significantly influence cell characteristics. As we shall see, these mechanisms generally tend to increase the excess currents J_E and J_{SCR} defined in Eqs. (4) and (5). They do so either by increasing the excess mobile charges, Q_E and Q_{SCR}, or by decreasing the related time constants, τ_E and τ_{SCR}.

The mechanisms to be discussed fall into two broad categories:

(a) Distortion of the energy-band edges and production thereby of effective gap shrinkage (or an effective intrinsic density) and quasi-electric fields. Gap shrinkage tends to increase the excess mobile charge, particularly Q_E. The quasi-electric fields can affect both excess mobile charge and the transit times, particularly in the emitter. These mechanisms alter Eqs. (11), (12), (17), and (18) of the basic set underlying the traditional analysis of solar cells.

(b) Alteration of the recombination rates (rates of interband transitions), denoted by R_n and R_p in Eqs. (14) and (15). This can directly influence the time constants τ_E and τ_{SCR}, and, through this influence, the excess mobile charges Q_E and Q_{SCR}.

We now discuss these two categories of mechanisms.

Effective Gap Shrinkage

At high doping concentrations, various deviations from the conventional band structure can occur, such as:

(a) The band edges need no longer be sharp; rather, states can extend beyond the band extrema describing lowly-doped silicon, forming thereby so-called band tails [12];

(b) The impurity states can broaden into an impurity band [13] with increasing impurity concentration; at high levels of doping these states can become delocalized;

(c) A spatial variation of the energy gap can result from macroscopic lattice strain introduced by a high-concentration diffused impurity profile, the strain arising from the misfit of the impurities in the silicon lattice [14].

As Figure A-2 illustrates qualitatively, each of these deviations tends to produce an effective shrinkage ΔE_G of the energy band gap. Because the intrinsic density n_i depends exponentially on the band gap, the gap shrinkage can be imbedded in an effective intrinsic density [15], which then appears directly in Eqs. (17) and (18) of the basic set. Note that spatial dependence of the doping concentration implies spatial dependence of the effective band gap.

To examine qualitatively the effect of gap shrinkage on the conduction processes described in Eqs. (11) and (12) of the basic set, we must distinguish between whether the states introduced by high doping are localized or delocalized. Thus, borrowing from the concepts used in models describing amorphous

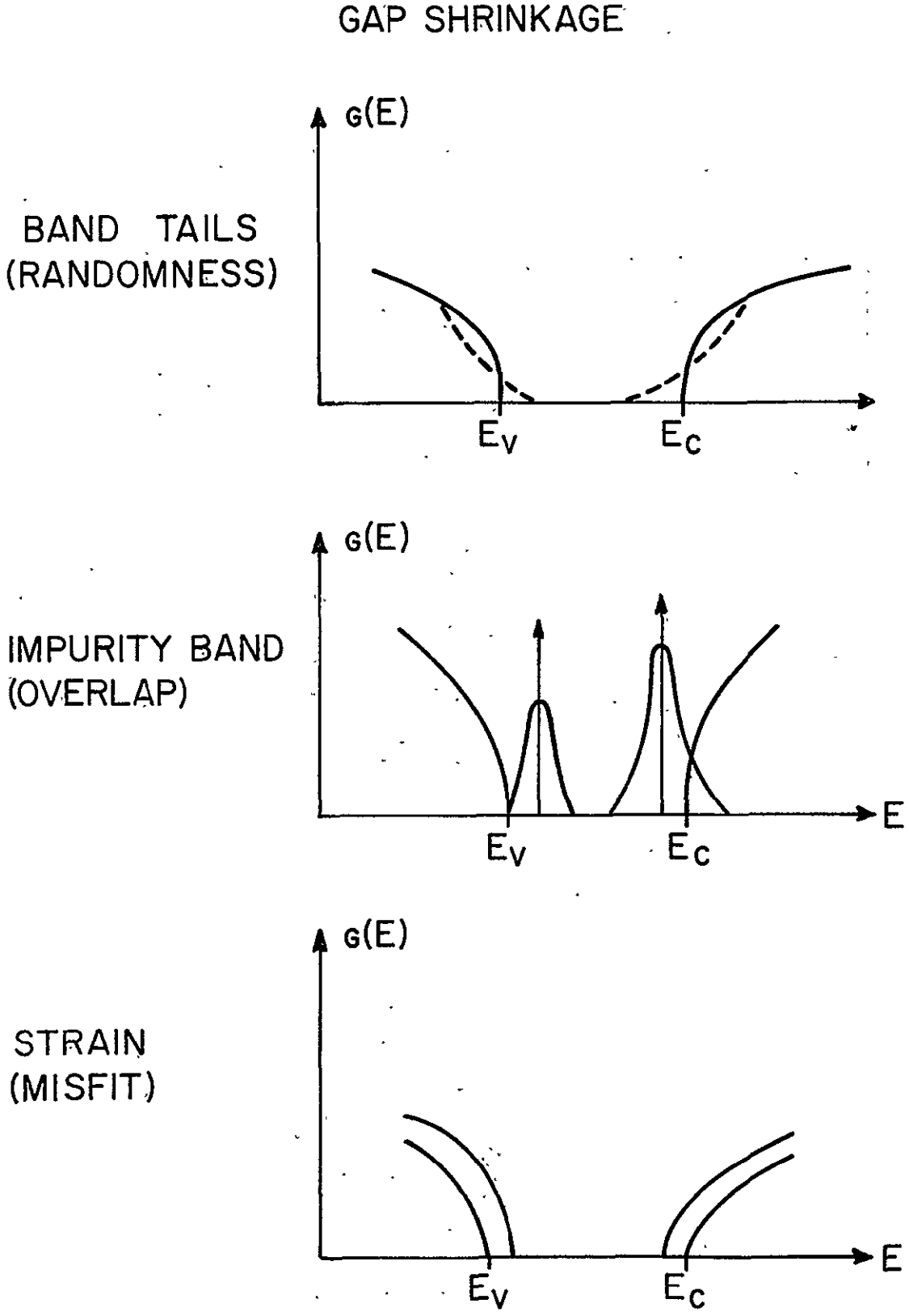

Fig. A-2 Qualitative suggestion of three sources of effective gap shrinkage.

semiconductors, we identify a critical energy, the Cohen mobility edge [16], which separates localized from delocalized states; the mobility edge plays a role in describing charge transport in disordered solids similar to that which the band edge plays in periodic solids such as lightly-doped silicon.

Then, for delocalized states, conduction can occur by drift and diffusion; if the variation in doping produces spatial dependence of the band gap or of the electron affinity, quasi-electric fields [17] can influence the transport of electrons and holes. For localized states, conduction can occur from hopping between neighboring states [18] due to thermally activated transfer of the trapped charges in the Mott model [19] or by tunneling in the Anderson model [20].

For ordinary temperatures, only the delocalized states will contribute appreciably to current flow. But, in such states, notice that three forces can act to produce the flow of holes and electrons: the statistical force due to diffusion and the Coulomb force due to the electric field--just as in lightly-doped silicon--plus the effect of the quasi-electric fields (another statistical force). Thus Eqs. (11) and (12) each require one additional term; however, Eqs. (11a) and (12a), in terms of the quasi-Fermi potentials, remain valid.

Interband Transition Rates (Recombination Rates)

Transitions between localized and delocalized states that constitute recombination-generation-trapping processes occur via several energy-momentum conservation mechanisms, including phonon-assisted, photon-assisted, and Auger-impact processes [21].

The rates of such transitions depend on the density of the defect centers, and the corresponding energy levels, capture cross sections and emission rate constants. By a combination of experimental methods [22], one can establish values for all of these in the junction space-charge region and the base of the cell. In the highly-doped emitter, one expects the defect density to rise sharply near the degenerately-doped surface. This expectation arises from the strong suggestion of experiment [23] that defects in silicon device processing are generated at the strained disordered surface layer, from where they diffuse rapidly into the bulk. These experiments further suggest that the defects are silicon vacancies or vacancy complexes. Thus, using the analogy to chemical reactions reviewed by Fuller [24], one finds the following first-order model for the *dependence of the defect density* N_{TT} *on the doping* N_D in the emitter and space-charge regions.

$$N_{TT}(x) = K[N_{DD}(x) + N_{AA}]^r \qquad (19)$$

which applies for sufficiently large N_D.

In deriving this model, one assumes approximate thermal equilibrium during the diffusion of impurities; this justifies the law of mass action, which one combines with the neutrality condition. The different values of the exponent r derive from different hypotheses about the dominant chemical reaction. For reactions corresponding to the formation of di-vacancies, for example, the choice $r = 2$ provides an approximate fit.

Aside from the processes mentioned one other kind exists that can influence the effective interband transition rates.

This kind involves tunneling via deep-level defect centers. Among the many processes of this general type [25], we shall describe here a particular two-step electronic process. This process assumes an electron in the conduction band is first captured by a localized deep level and subsequently tunnels to the valence band or to the valence-band tail states; Sah has demonstrated this as the excess-current mechanism in gold-doped silicon tunnel diodes [25].

QUALITATIVE REMARKS ABOUT WHICH MECHANISM DOMINATES

Consider first the physical mechanisms that affect the interband transition rates. In the quasi-neutral substrate (the base) of the cell, description of these rates by a simple lifetime, assumed *spatially independent*, may suffice as a first-order approximation, although experimental evidence is wholly lacking at present. We make this assumption for simplicity. In the junction space-charge region, the simplest model, due to Sah, Noyce and Shockley [26], assumes that electronic transitions between the conduction and valence band occur via localized states of a single energy level lying deep within the forbidden band. These two processes produce the base current and the SCR current of the traditional analysis, as defined in Eqs. (3) and (4).

By physical reasoning, one can see what conditions tend to yield dominance of one of these currents over the other. The base current results from carriers that have surmounted the entire barrier of the junction region. To contribute to the SCR current, however, the carriers need to have climbed only part of

the barrier. Therefore any conditions that increase the barrier height or decrease the climbing energy of the carriers tend to cause dominance of SCR current. Hence the dominance of SCR current is more likely for loads approximating short-circuit rather than open-circuit conditions and for lower rather than higher temperatures. For very low temperatures, one may see the appearance of the processes [25] that involve tunneling, because tunneling enables holes and electrons to reach nearly the same spatial position without needing to climb the barrier. A steep junction also favors tunneling processes.

In the quasi-neutral diffused layer (emitter), Auger processes may compete significantly with Shockley-Read-Hall (SRH) processes near the surface, where majority carriers exist in great numbers. Near the edge of the junction space-charge region, where doping is relatively low, our calculations indicate that SRH processes will dominate *band-to-band Auger processes*. For the present, the relative role of *Auger recombination via defect centers* cannot be assessed because of the absence of experimental studies that would fix the values of the pertinent rate constants.

Consider now effective gap shrinkage and its characterization. Recently strides have been made toward including the effects of gap shrinkage (often characterized by an effective intrinsic density) in explaining the operation of a bipolar transistor [27]. From this inclusion has come a closer agreement between experiment and theoretical prediction than was obtained previously, particularly for the forward-active current gain and the gain-bandwidth product. This suggests direct

applicability to solar cells of the model for gap shrinkage used in transistor theory; but uncertainties exist that call for caution.

The model for gap shrinkage now used in bipolar transistor theory is based, essentially, on the Kleppinger-Lindholm extrapolation [28] of the characterization of Morgan [13] for impurity-band widening and of Bonch-Bruyevich [12] for band tailing. No direct experimental evidence has yet appeared to assess the degree of fit for silicon of the theories of Morgan and Bonch-Bruyevich; and Kleppinger and Lindholm intended their extrapolation to serve only as a first-order approximation. Further, the usage put to this extrapolation in the computation of transistor behavior has evolved quite different dependencies of the effective intrinsic density (or effective gap shrinkage) on the doping density. This one can see by comparing dependencies appearing in the various treatments [27]. Finally, the theory treats the states in the Kleppinger-Lindholm extrapolation all as delocalized states. This adds to the exaggeration of gap shrinkage inherent already in the extrapolation.

Thus first-order models for gap shrinkage exist that probably could bring the predicted and measured performance of cells into better accord. But we conclude that the uncertainties present in the existing theories rule out for the present a definitive inclusion of the effects of this mechanism. In assessing the relative significance of gap shrinkage, therefore, we shall try to evade the uncertainties of the existing theories by relying on simple estimates. This possibility we explore in the next section.

EXTENSIONS OF THE TRADITIONAL ANALYSIS

Here we extend the method of the traditional analysis to estimate the effects of spatially-dependent gap shrinkage and recombination rates. We do this for a cell of 0.1 ohm-cm resistivity operating at a temperature of $300^{o}K$. For such a cell at this temperature, consistent with our discussion in the foregoing section, we anticipate that gap shrinkage and altered recombination will be the significant additional mechanisms acting to determine cell performance. Our interest in a 0.1 ohm-cm cell arises from the maximum it shows in measured open-circuit voltage [3]. For concreteness, we assume a phosphorous-diffused n+p cell with a surface concentration of $10^{20}cm^{-3}$ and a junction depth of 0.25 microns.

As in the traditional analysis, we regard the current at the terminals as the sum of J_L and J_D in accord with Eq. (1). Because gap shrinkage occurs appreciably in the emitter region only, which constitutes a small fraction of the volume of the entire cell, we assume that gap shrinkage negligibly affects J_L. Thus we use the traditional value for J_L [9] applicable to semi-infinite bulk material.

As in Eq. (2), we regard J_D as the sum of three components, and we now seek to calculate these. According to Eqs. (3) - (5), this involves calculation of the excess mobile charge and the time constant characterizing each of the three regions of the device.

The Base Region

Treatment of the substrate (base) region requires no changes from traditional analysis. Consistent with experimental data on diffused devices [23], we *assume* a spatially-independent defect density and lifetime τ_B in the region; and, consistent with theories of gap shrinkage [28], we assume negligible shrinkage for a doping concentration, $N_{AA} = 5(10^{17})$ cm^{-3}, which corresponds to p-type resistivity of 0.1 ohm-cm. Thus,

$$J_B = \frac{Q_B}{\tau_B} = \frac{[qL_B(n_i^2/N_{AA}\ \exp(qV/kT)]}{\tau_B} \qquad (20)$$

Substitution of $L_B \simeq 10$ microns, which is consistent with recent data [9] for diffusion length L_B against doping,* and combination with Eq. (10) then yields

$$V_{OC} \simeq 680 \text{ mV} \qquad (21)$$

This agrees satisfactorily with the predictions of traditional theory [3]*; the maximum measured value is 610 mV [3].

---

* There is scatter in these data of about one order of magnitude for a resistivity of 0.1 ohm-cm. Use of 100 microns in this calculation would yield an open-circuit voltage of about 740 mV, which would not change qualitatively the conclusions to be drawn.

Junction Model

Now consider the junction space-charge region. At open-circuit conditions the junction barrier is forward biased by a voltage approximating V_{OC}. According to depletion theory, the width W_{SCR} of the junction space-charge region narrows to a value lower than its width at thermal equilibrium. As a first-order approximation in calculating W_{SCR}, we shall assume a linear junction space-charge region; that is,

$$N_{DD} - N_{AA} = -a(x-x_j) \tag{22}$$

For junctions formed by the conventional processing used in transistor fabrication, the doping gradient "a" does not exceed about 10^{23} cm^{-4}, according to recent measurements on shallow phosphorous-doped emitter junctions [29]. For junctions formed by the lower-temperature processing used in solar-cell fabrication, we assume this value constitutes a reasonable upper bound for the doping gradient.

In bipolar transistor theory, a linear junction model [8,30] is often used as an approximation for the emitter junction [29,31,32], even for devices with very shallow and heavily doped emitters. This approximation serves as a better model for solar-cell junctions than does the step-junction approximation commonly used, because a step junction can severely exaggerate the influence of gap shrinkage on cell behavior, as the discussion to follow will imply.

The linear-junction approximation itself, however, proves incapable of providing good estimates of various aspects of behavior; for example, it underestimates the strength of the

built-in field and the doping density at the emitter edge of the space-charge region. Thus, where needed in the course of the treatment below, we shall indicate certain refinements of this approximation.

Extensions for the Junction Space-Charge Region

Assuming a linear junction, we now use conventional calculations of W_{scr} which derive from solution of Poisson's equation *under the depletion approximation*. For a doping gradient of 10^{23} cm^{-4}, these yield at T = 300°K

$$W_{SCR} \simeq 1000A°$$

which decreases to about half of this value for

$$V \simeq V_{OC} \simeq 610 \text{ mV}.$$

The thinning is less than this because the presence of mobile carriers invalidates the depletion approximation [30]. Moreover, the asymmetrical departures of the actual profile from that of Eqn. (22) imply that less than one-half of the total thickness of the space-charge region occurs on the emitter side of the metallurgical junction. But we content ourselves with estimates here, recognizing that several Debye lengths (which mark the width of the blurs separating space-charge and quasi-neutral regions) occupy several hundred Angstroms of material for the doping levels of interest.

Using the estimate $W_{SCR} = 1000$ A°, together with the assumption of a linear junction and of "a" = 10^{23} cm^{-4}, we find the maximum value of the doping in the space-charge region:

$$N_D(x_E) \simeq 10^{18} \text{ cm}^{-3} \qquad (23)$$

in which x_E denotes the boundary separating the quasi-neutral emitter from the space-charge region. This constitutes a lower-bound estimate because the profile on the emitter side of the rises more rapidly than does the linear profile of Eqn. (22); and, as shown by calculations based on a piece-wise linear approximation of the actual profile, the maximum density may be as much as twice that given in Eqn. (23). Neither experimental evidence [33] nor theory [28], however, suggests appreciable gap shrinkage for doping concentrations less than $2(10^{18})cm^{-3}$; and thus we neglect this mechanism in the junction space-charge region. This neglect, which the treatment in the next section substantiates in more detail, is one central consequence and simplification yielded by the linear-junction model and its piece-wise linear refinement.

According to Eq. (19), however, the defect density and hence the lifetime can vary significantly with position in the space-charge region. In using Eq. (19) to demonstrate this, we assume it to be valid also for small N_D. This additional approximation simplifies the estimates to be made and allows a one-parameter fit to data. From a physical standpoint, it has the drawback, however, of suggesting the same kind of defect predominates in the bulk as near the surface, which is questionable [23]. To simplify the estimates further, we assume the lifetime varies inversely with the defect density; this approximation probably introduces only small error in the absence of significant Auger recombination via traps.

Thus, in the space-charge region,

$$\frac{N_{TT}(x)}{N_{TTB}} = \frac{\tau_B}{\tau_{SC}(x)} = \frac{[N_{DD}(x) + 5(10^{17})]^r}{5(10^{17})} \qquad (24)$$

This dependence is shown qualitatively in Figure A-3 with $N_{DD}(x)$ given by Eq. (22). The maximum value of this ratio occurs at the emitter edge of the space-charge region, and is 3^r, which implies about an order of magnitude decrease in lifetime for r=2 and two orders of magnitude for r=4. A simple linear average across the width of the space-charge region produces the following values for the ratio $\tau_B/\langle\tau_{SC}\rangle$: 2 for r=1, 3 for r=2, 7 for r=3; and 16 for r=4.

To specify the current J_{SC}, we identify the pertinent charge Q_{SC} from the Sah-Noyce-Shockley theory [26] and choose an appropriate average lifetime τ_{SC} for the region:

$$J_{SC} = \frac{Q_{SC}}{\tau_{SC}} \simeq \frac{[qn_i W_{SC}]\exp[qV/2kT]}{\tau_{SC}} \qquad (25)$$

For the current density J_{SC} in this cell, the main departure from traditional theory caused by heavy doping in a one-dimensional model results from the rise in defect density and fall of lifetime near the highly-doped surface.

Extensions for the Emitter Region

The quasi-neutral emitter region (diffused layer) of the cell under study contains very high doping concentrations. Nonetheless, we shall indicate that the resultant gap shrinkage *in a one-dimensional model* fails to give enough deviation from traditional predictions to fit empirical data, whereas spatially-dependent lifetime does suffice. This suggests that, for the cell under

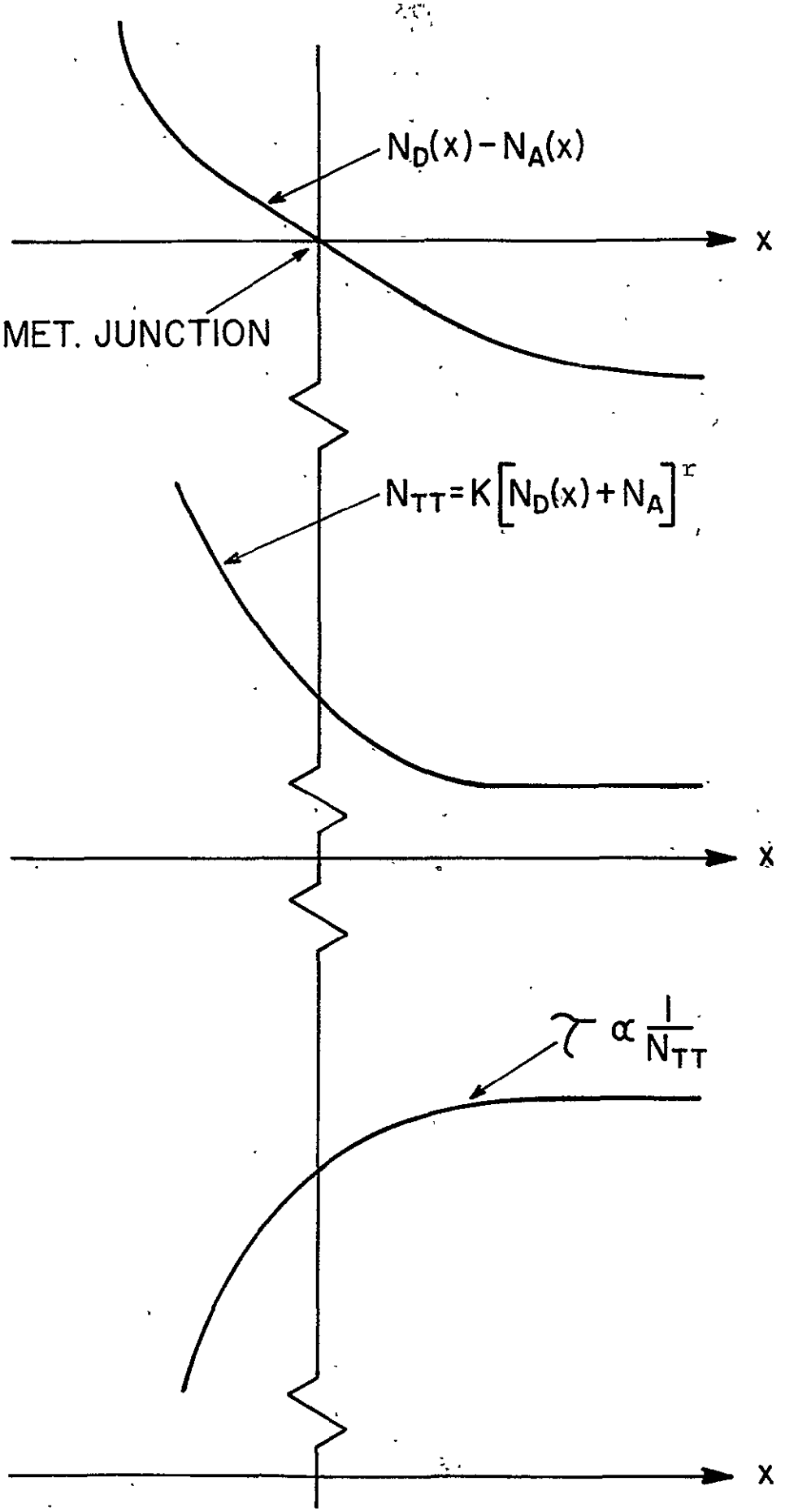

Fig. A-3 Qualitative suggestion of sharp rise of defect density and sharp fall of lifetime near the surface.

consideration, at a temperature of 300°K, the main additional mechanism *in a one-dimensional model* governing J_E of the emitter is spatially-dependent lifetime.

Our approach here will involve estimating *upper bounds* on the gap shrinkage possible. The upper bounds to be used will depend strongly on the spatial distribution of the holes in the emitter, and our treatment will start with that issue.

The key insight lies in recognizing that the built-in electric field produced by the doping gradient in the emitter packs the minority carriers (holes) very near the space-charge-region edge. Kennedy and Murley [31] were the first to identify this compression as a main contributor to the injection efficiency of bipolar transistors.

Their calculations are based on a refinement of the linear junction model whose power-series approximation to the profile of the emitter side of the metallurgical junction is meant to provide a good estimate of the built-in electric field in the quasi-neutral emitter. The calculations show the holes confined close to the space-charge edge x_e, within a region ten percent of the thickness of the entire quasi-neutral emitter. Specifically, they show that within this region the hole density drops by an order of magnitude from the value $p(x_e)$ at the edge of the space-charge region. It drops with the spatial distribution shown qualitatively in Figure A-4, which implies that practically all holes vanish within a region thirty percent of the emitter thickness.

Although the calculations apply to a device different from the cell under study, the differences further support the contention

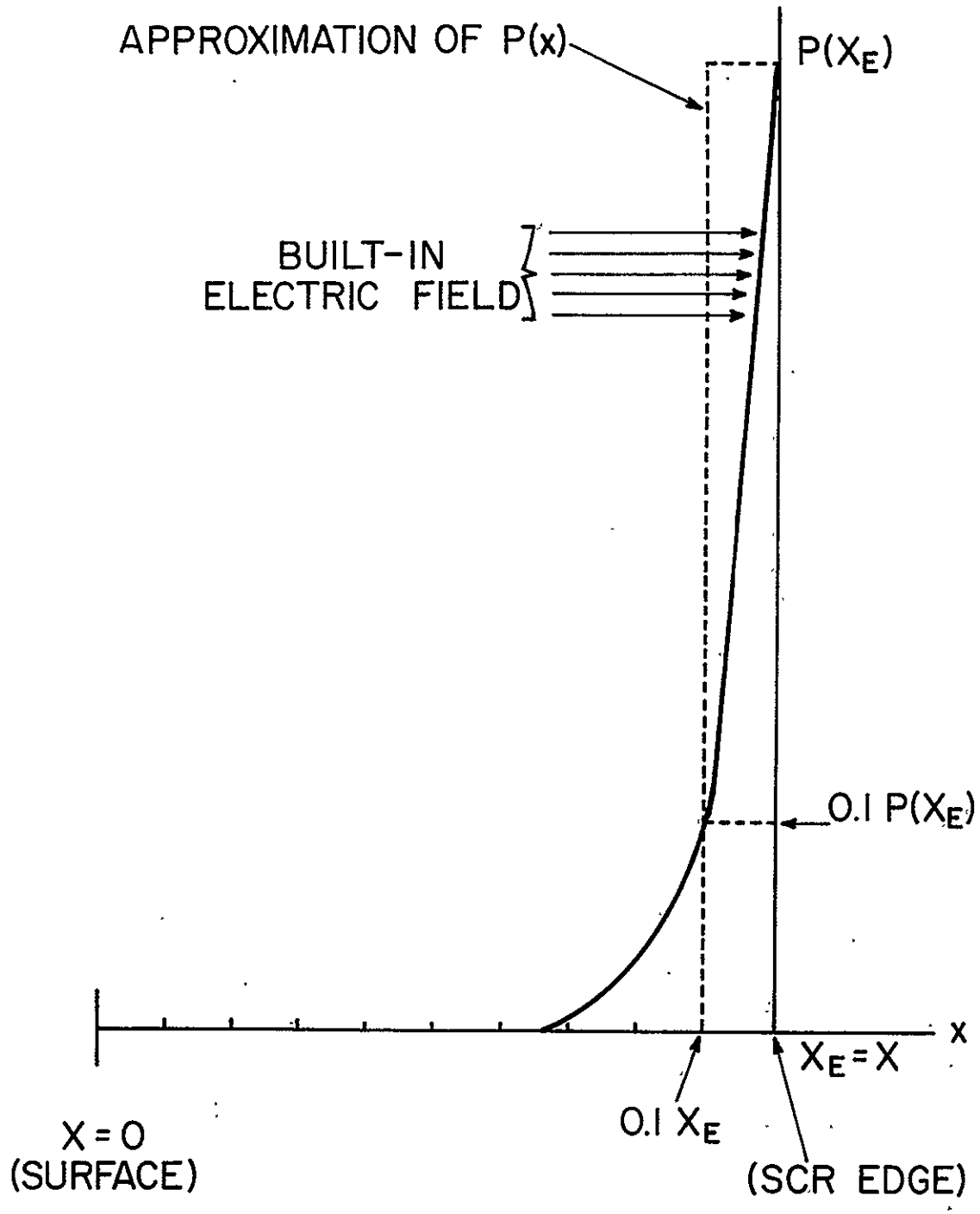

Fig. A-4 Approximate distribution of minority carriers in quasi-neutral diffused layer (emitter) of dark cell (assuming the quasi-fields are negligible near x_E where N_D is relatively small).

that the holes exist in appreciable numbers only in a thin region near x_e. Kennedy and Murley assumed a junction depth x_j = 1.75 microns, considerably deeper than the value x_j = 0.25 microns assumed here. But a shallower junction and consequent higher built-in field would only tend to compress the holes more tightly. Kennedy and Murley assumed a spatially-independent lifetime, and a lifetime that varies in accord with Eq. (19) would again only add to the compacting.

Thus we conclude that the holes in the emitter of the cell occupy at most ten percent (200 A°) of the quasi-neutral emitter, and are *confined to the lowest-doped region of the emitter*. In all regions of the dark cell significant to its performance, therefore, *gap shrinkage is small*.

To place an upper bound on the effects of gap shrinkage, we assume the rectangular distribution shown dashed in Figure A-4. This distribution conflicts with the demands of hole diffusion, but it is meant only to clarify which mechanism dominates rather than as a tool for decisive calculation. For the thickness of the base of the rectangle, we choose L_E = 200A° consistent with the discussion above and recognizing that this choice corresponds to about two Debye lengths for this doping; hence choice of a smaller value obscures physical meaning.

In this region of hole occupancy in the emitter, if we continue to assume the linear-junction model of Eq. (22), we find that N_{DD} will have risen to $1.2(10^{18})$ cm^{-3} at x'_E, which defines the edge of the hole distribution nearest the surface. As discussed in the foregoing section, a piece-wise linear approxima-

tion to the doping profile implies $N_{DD}(x_E') \simeq 2(10^{18})/cm^3$, which we choose for subsequent calculations.

Estimation of J_E from Eq. (5) requires estimation of Q_E and τ_E. For Q_E, we extend conventional theory by inserting in the customary expression for $n_i(x_E')$ a band gap altered by the shrinkage $\Delta E_G(x_E)$. Thus,

$$Q_E = \{qL_E n_i^2(x_E')/[N_D(x_E) - N_A]\}e^{qV/kT}$$

$$= \frac{qL_E n_i^2}{N_D(x_E) - N_A} e^{\Delta E_G(x_E')/kT} e^{qV/kT} \qquad (26)$$

To give an upper bound for $\Delta E_G(x_E')$, note the empirical evidence of Pearson and Bardeen [33] that the ionization energy of shallow dopants in silicon vanishes for concentrations between 10^{18} and 10^{19} cm^{-3}. As a rough estimate, we interpret this to imply that the conduction band extends downwards by the ionization energy of phosphorous: $\Delta E_C = 0.044$ eV. We add this with Fritzche's description of band-tail states [34]--giving a shift upwards of the valence band of $\Delta E_V \simeq 0.025$ eV. This yields $\Delta E_G(x_E') \simeq 0.07$ eV $\simeq 2.7kT$ and $\exp(\Delta E_G(x_E')/kT) \simeq 15$.

To estimate $\tau_E(x_E')$, we use the reasoning of the foregoing subsection, adding the consideration that the assumed shift ΔE_V in the effective valence band increases the hole capture cross section by about a factor, $\exp(\Delta E_V/kT) \simeq e$. Thus,

$$\tau_B/\tau_E(x_E') \simeq e(5)^r \qquad (27)$$

which gives: 14 for r=1; 68 for r=2; 340 for r=3; 1700 for r=4. This departure from traditional theory compares to the upper-bound estimate of 15 for the departure arising from gap shrinkage.

In accord with Eq. (5),

$$J_E = \frac{qn_i^2 x_E}{[N_D(x_E) - N_A]\tau_B} e^{qV/kT} \times [L_E/x_E]$$

$$\times [\exp \frac{\Delta E_G(x_E')}{kT}] \times [e(5)^r]$$

$$= J_{ET} FGS \qquad (28)$$

The first term J_{ET} is the J_E for a shallow-junction cell that results from application of traditional theory to an abrupt-junction model. The next three terms are correction factors arising from three different physical mechanisms: The first of these F, whose value is approximately F = 0.1, accounts for the compacting of the hole density by the built-in electric field. The second G, which has an upper bound G=15, accounts for gap shrinkage. The last S accounts for a spatially-dependent lifetime, and has the values listed above for different values of r.

Implications of Measured V_{OC}

From a physical point of view, the open-circuit voltage arises to establish J_D just large enough to balance J_L. Of the three components of J_D, J_{SC} will be highly significant at lower temperatures, for the reasons noted earlier. For T = 300°K, calculations based on our previously stated assumptions show it to be less than J_B for $V = V_{OC}$. Thus we ignore J_{SC} for the present discussion.

From Eq. (10), therefore, to fit empirical data,

$$J_{OE} + J_{OB} = \exp(q\Delta V_{OC}/kT) J_{OB} \qquad (29)$$

implying

$$J_{OE} \simeq 14 J_{OB} \qquad (30)$$

Here ΔV_{OC} denotes the difference between the measured value of 610 mV and the theoretical value of 680 mV calculated from traditional theory assuming $J_B >> J_E$. J_{OB} and J_{OE} denote the saturation currents for J_B and J_E.

Combining Eqs. (20) and (28) gives:

$$J_{OE}/J_{OB} = (J_{OET}/J_{OB})FGS \tag{31}$$

where

$$J_{OET}/J_{OB} = x_E/L_B \simeq 0.02 \tag{32}$$

is the ratio predicted by traditional theory and FGS represents the correction factor arising from the three physical mechanisms described earlier. To fit empirical data, FGS ≃ 700.

The factor F, representing the effect of the built-in electric field in the emitter, is approximately

$$F = L_E/x_E \simeq 0.1$$

The factor G, which accounts for the effects of gap shrinkage, has an upper bound of 15. To fit the data, therefore, the factor S, which describes the influence of spatially-dependent lifetime, must be at least 466. This implies an exponent r=3 in Eq. (19) describing the rise of the defect density near the surface. The Sah-Wang experiments [23] concerning defects from silicon-device processing suggest that vacancy complexes could give rise to the defects observed, which is consistent with this value of r. Several considerations combine, however, to suggest that smaller values of r, and thus less complex configurations of the defects, will suffice to bring theoretical and empirical V_{OC} into conformity. First, if Auger recombination *via traps* preponderates in determining

the recombination for a doping density of $2(10^{18})/cm^3$, then the needed value shifts to $r \leq 2$, which suggests di-vacancies as a possible defect configuration. Lack of experimental data about the pertinent rate constants rules out a quantitative assessment of this possibility; the data available, however, indicate that *band-to-band* Auger processes play a second-order role in the device under study. Second, if the processing used to form the junction were to depress $\tau_B(x)$ below its pre-processing value, this also would drive down the needed value of the parameter r. Finally, areal inhomogeneity, discussed in Section III, would produce the same tendency.

Note that band-gap shrinkage alone cannot explain the data. Even if the upper-bound estimate of its influence is assumed, a factor of 466 still separates experiment and theory. From a physical point of view, this occurs because for the dark cell under study essentially no holes are present in regions where the gap shrinkage might be appreciable.

For this cell, subject to the validity of the assumptions made, the additional physical mechanism determining V_{OC} in this *one-dimensional* model for high-doping limitations is dominantly the drop in lifetime near the surface.

REFERENCES FOR APPENDIX A

1. H.W. Brandhorst, Jr., Record of 9th Photovoltaic Specialists Conf., 1 (1972).

2. M. Wolf, Record of 10th Photovoltaic Specialists Conf., 5 (1973).

3. M.P. Godlewski and H.W. Brandhorst, Jr., "Effects of High Doping Levels on Silicon Solar Cell Performance," High Efficiency Silicon Solar Cell Meeting, NASA-Lewis Research Center, Nov. 1974.

4. J.G. Fossum, "Computer-Aided Analysis of Silicon Solar Cells," Sandia Labs. Report SLA-74-0273 (1974).

5. P.M. Dunbar and J.R. Hauser, Paper 1.2, 11th Photovoltaic Specialists Conf. (1975); see this Record.

6. P.M. Dunbar and J.R. Hauser, "A Study of Efficiency in Low-Resistivity Silicon Solar Cells," Solid State Electronics (accepted for publication).

7. R.J. Stirn, Record of 9th Photovoltaic Specialists Conf., 72 (1972).

8. W. Shockley, Bell Syst. Tech. J., 28, 435 (1949).

9. S. Soclof and P.A. Iles, Junction Effects in Silicon Solar Cells, Final Report, NASA Contract NAS 3-17360, Centralab Semiconductor Div., El Monte, Calif. (in press).

10. W. Shockley and W.T. Read, Phys. Rev., 87, 835 (1952).

11. R.N. Hall, Phys. Rev., 87, 387 (1952).

12. I.M. Lifshitz, J. Exp. Theor. Phys., 2, 117, 137, 156 (1942); V.L. Bonch-Bruyevich and A.G. Mironov, Soc. Phys. Solid State, 3, 2194 (1962); E.O. Kane, Phys. Rev., 131, 1532 (1963).

13. G.W. Castellan and F. Seitz, Phys. Rev., 79, 216 (1950); C.S. Hung, Phys. Rev., 79, 727 (1950); C. Ererginsoy, Phys. Rev., 80, 1104 (1950); T.N. Morgan, Phys. Rev., 139, A343 (1965).

14. V. Fistful, Heavily Doped Semiconductors, Plenum Press, N.Y. (1969).

15. H.J.J. DeMan, IEEE Trans. on Electron Devices, ED-18, 833 (1971).

16. M.H. Cohen, H. Fritzsche, and S.R. Ovshinsky, Phys. Rev. Lett., 22, 1065 (1969).

17. H. Kroemer, RCA Review, 333 (1957).

18. E.M. Conwell, Phys. Rev., 103, 51 (1956).

19. N.F. Mott, Can. J. of Physics, 34, 1356 (1956).

20. P.W. Anderson, Phys. Rev., 109, 1492 (1958).

21. See references in: C.T. Sah, Physica Status Solidi a, 7, 541 (1971).

22. C.T. Sah, L. Forbes, L.L. Rosier, and A.F. Tasch, Solid State Electronics, 13, 259 (1970);
C.T. Sah, W.W. Chan, H.S. Fu and J.W. Walker, Appl. Phys. Lett., 20, 193 (1972);
L.D. Yau and C.T. Sah, Appl. Phys. Lett., 22, 157 (1972);
C.T. Sah and J.W. Walker, Appl. Phys. Lett., 22, 384 (1973).

23. C.T. Sah and C.T. Wang, J. Appl. Phys., 46, 1767 (1975).

24. C.S. Fuller, Ch. 5 in N.B. Hannay ed., Semiconductors, Reinhold Corp., N.Y., 1959.

25. C.T. Sah, Phys. Rev., 123, 1594 (1961).

26. C.T. Sah, R.N. Noyce, and W. Shockley, Proc. IRE, 45, 1228 (1957).

27. R.J. Van Overstraeten, H.J. DeMan and R.P. Mertens, IEEE Trans. on Electron Devices, ED-20, 290 (1973);
H.J. De Man, R.P. Mertens and R.J. Van Overstraeten, Electronic Letters, 9 (1973);
R.P. Mertens, H.J. De Man and R.J. Van Overstraeten, IEEE Trans. on Electron Devices, ED-20, 772 (1973);
M.S. Mock, Solid-State Electronics, 16, 1251 (1973);
M.S. Mock, Solid State Electronics, 17, 819 (1974).

28. D.D. Kleppinger and F.A. Lindholm, Solid-State Electronics, 14, 199-206, 407-416 (1971).

29. J.A. Kerr and F. Berz, IEEE Trans. Electron Devices, ED-22, 15 (1975).

30. C.T. Sah, Proc. IRE, 49, 603 (1961).

31. D.P. Kennedy and P.C. Murley, IRE Trans. Electron Devices, ED-9, 136 (1962).

32. D.J. Roulston, Solid State Electronics, 18, 427 (1975).

33. G.L. Pearson and J. Bardeen, Phys. Rev., 75, 865 (1949).

34. H. Fritzche, Ch. 5 in J. Tauc (ed.), Amorphous and Liquid Semiconductors, Plenum Press (1972).

35. W. Shockley, Solid-State Electronics, 2, 35 (1961).

APPENDIX B: PAPERS AND REPORTS DERIVING FROM THE SUPPORT OF GRANT NSG-3018

1. F.A. Lindholm, S.S. Li, and C.T. Sah, "Studies of Some Fundamental Limitations of the Performance of PN Junction Silicon Solar Cells," High Efficiency Silicon Solar Cell Meeting, NASA Lewis Research Center, November 1974.

2. S.S. Li, F.A. Lindholm, P.J. Chen, and C.T. Sah, "Experimental Studies of Defect Centers in Low Resistivity Silicon PN Junction Solar Cells," High Efficiency Silicon Solar Cell Meeting, NASA Lewis Research Center, November 1974.

3. F.A. Lindholm, S.S. Li, and C.T. Sah, "Studies of Silicon PN Junction Solar Cells : Semi-Annual Status Report," January 1975.

4. F.A. Lindholm, S.S. Li, and C.T. Sah, "Fundamental Limitations Imposed by High Doping on the Performance of PN Junction Silicon Solar Cells," Record of Eleventh IEEE Photovoltaic Specialists Conference 75CH0948-OED, pp. 3-12 (1975).

5. F.A. Lindholm, S.S. Li, and C.T. Sah, "Process-Induced Defects in Terrestrial Solar Cells," National Photovoltaic Program Review Meeting, Los Angeles, July 1975 (paper invited by United States Energy Research and Development Administration).

APPENDIX C: PERSONS WORKING ON THE RESEARCH OF GRANT NSG-3018

I. Faculty (University of Florida)

Dr. F.A. Lindholm, principal investigator

Dr. S.S. Li

II. Other Faculty (University of Illinois)

Dr. C.T. Sah

III. Graduate Students

P. Chen

S. Pao

J. Weichbrodt